



**HAL**  
open science

## Assessing crack initiation and propagation in flax fiber reinforced clay subjected to desiccation

Ahmad El Hajjar, Tariq Ouahbi, Said Taibi, Joanna Eid, Mahdia Hattab,  
Jean-Marie Fleureau

### ► To cite this version:

Ahmad El Hajjar, Tariq Ouahbi, Said Taibi, Joanna Eid, Mahdia Hattab, et al.. Assessing crack initiation and propagation in flax fiber reinforced clay subjected to desiccation. *Construction and Building Materials*, 2021, 278, pp.122392. 10.1016/j.conbuildmat.2021.122392 . hal-03251225

**HAL Id: hal-03251225**

**<https://hal.univ-lorraine.fr/hal-03251225>**

Submitted on 13 Feb 2023

**HAL** is a multi-disciplinary open access archive for the deposit and dissemination of scientific research documents, whether they are published or not. The documents may come from teaching and research institutions in France or abroad, or from public or private research centers.

L'archive ouverte pluridisciplinaire **HAL**, est destinée au dépôt et à la diffusion de documents scientifiques de niveau recherche, publiés ou non, émanant des établissements d'enseignement et de recherche français ou étrangers, des laboratoires publics ou privés.



Distributed under a Creative Commons Attribution - NonCommercial 4.0 International License

# Assessing crack initiation and propagation in flax fiber reinforced clay subjected to desiccation

Ahmad El Hajjar<sup>1</sup>, Tariq Ouahbi<sup>1,\*</sup>, Said Taibi<sup>1</sup>, Joanna Eid<sup>1,2</sup>, Mahdia Hattab<sup>3</sup>, Jean-Marie Fleureau<sup>4</sup>

<sup>1</sup> Normandie University, UNIHAVRE, Laboratory of Waves and Complex Media, UMR 6294 CNRS, Le Havre, France.

<sup>2</sup> Holy Spirit University of Kaslik (USEK), Civil Engineering Department, Jounieh, Lebanon.

<sup>3</sup> Université de Lorraine, Laboratoire d'Etude des Microstructures et de Mécanique des Matériaux, UMR 7239 CNRS, Arts et Métiers ParisTech, Metz, France

<sup>4</sup> Université Paris-Saclay, CentraleSupélec, Laboratoire de Mécanique des Sols, Structures et Matériaux, UMR 8579 CNRS, Gif-sur-Yvette, France.

\* Corresponding Author.

E-mail: [tariq.ouahbi@univ-lehavre.fr](mailto:tariq.ouahbi@univ-lehavre.fr) ([Dr. Tariq Ouahbi](#))

## Abstract

Nowadays, raw earth construction is an area of growing interest, both for its eco-friendly characteristics and very interesting thermo-hygroscopic properties. Nevertheless, this type of construction exhibits a weakness related to cracking due to the shrinkage strains caused by desiccation. In this context, this paper presents an experimental study of restrained drying-shrinkage, carried out on a fine clayey soil. Several amounts of soil reinforcement with orderly layout patterns using vegetal flax fibers have been investigated in order to enhance soil properties. The new feature of this work is the analyzing of crack initiation and propagation by coupling the Digital Image Correlation (DIC) method with the Clay-Ring-Test (CRT) technique, using an innovative device called DIC-CRT. Suction measurements in clay samples are performed during desiccation using tensiometers. A good agreement is noticed between suction and strain evolution until cracking revealing the direct influence of suction on clay shrinkage. Through the two techniques, DIC and CRT, a relevant parameter to

quantify crack intensity in materials is proposed. A significant decrease of crack ratio, by a factor of about 8, highlights the impact of soil reinforcement on the level of crack opening. Likewise, a significant decrease, by a factor of about 20, is observed in the analysis of DIC and CRT slopes, highlighting the impact of reinforcement on the kinetic of crack opening.

**Keywords:** Raw earth building material; Clay soil; Flax fibers; Digital Image Correlation; Clay-Ring-Test; Plastic shrinkage; Desiccation cracking.

## **I – INTRODUCTION**

There is an awareness at the world level that natural and non-renewable resources are running out and that they are not going to last forever. This implies the existence of a primary need for more environmentally friendly materials. In this context, eco-materials based on raw earth, possibly reinforced with vegetal fibers, constitute one of the promising research prospects for the future of building materials [1].

Raw earth contains clayey soils, which are characterized by a consequent variation in volume when they are subjected to a high level of suction [2]. During desiccation, defined as the loss of water by evaporation, the clayey soil becomes unsaturated and a volume change occurs as long as the soil water content remains above the shrinkage limit. This volume change results in a shrinkage of the material. As a result, cracks appear and propagate. Therefore, evaporation takes place through the surfaces created by the cracks in addition to the soil surface [3]. This has consequences for hydraulic, mechanical and thermal properties, especially concerning water retention capacity, permeability and mechanical strength [4, 5].

Several authors studied shrinkage and cracking phenomena in clay materials in the literature. These works were interested in the comprehension of the mechanisms which govern the phenomenon of shrinkage and cracking, the origin which induces initiation of cracks, as well as the investigation of the network of cracks through several parameters such as: area of crack

and crack rate [6-22]. To achieve that, various techniques developed in laboratory to follow the displacements and strains evolution in the soil over the drying process have been set up. One of the most promising techniques is DIC (Digital Image Correlation).

DIC is a method based on non-contact optical technique that measures displacements and strains [23]. DIC is cost effective compared to other techniques such as speckle photography and interferometry, for optical characterization in soil's cracking. However, its use in soils field requires a rigorous calibration. This technique measures in the studied area the displacement of different patterns and identify the 2D or 3D transformations between reference and deformed digital images, through the principle of optical flow conservation.

Initially, a local method called DIC [24] was developed from 1980s. This method was developed in the basis of the application of the cross-correlation function, in which every image is split into several subsets. The positions of the subsets are then recognized in the deformed pictures relative to the reference picture. From the 2000s, a method called "global method" was developed. The basis of this method is the use of finite element method. The global method reduces the overall correlation residues [25], and performs smoother correlation by seeking a field of displacement that maintain grayscale in the picture [26].

In the field of geotechnical engineering, DIC method was used to investigate the behavior of several mixtures of montmorillonite and kaolinite spanned on a rectangular plate [17]. The results show that cracks occur following different more or less complex failure modes. In addition, Wei et al. [17] have noticed that, the propagation of the crack due to tension occurs at a direction perpendicular to the extensions. Eid et al. [18] used DIC to underscore the desiccation of a natural silt. Their results showed that the soil submitted to drying on a smooth support produces a uniform overall shrinkage up to cracking occurrence, though a localized heterogeneous deformations were observed. The shrinkage behavior of a concrete of raw earth mixed with various percentages of crushed concrete aggregates was studied by Kanema et al.

[19]. They established that incorporating water reducers decreases the crack appearance by reducing localized deformation and increasing the global one. In order to analyze the shale behavior on drying and wetting cycles, Wang et al. [27] used DIC technique and found that the assessing of the fields strain makes it possible of the initiation prediction of drying cracks. Ameer et al. [20] integrated the DIC method to a bending test on kaolin clay samples submitted to different suction levels. They showed that a critical deformation has been obtained once the stress reached the maximum tensile strength. Moreover, in order to assess the influence of edge effects on the cracking of kaolinite or montmorillonite materials using the DIC technique, El Hajjar et al. [28, 29] notified that in the case of a free shrinkage, it is possible that the kaolinite cracks by shear type deformations.

Another technique, called Ring-Test, was used to study the shrinkage stress. The Ring-Test is an experimental method widely used for assessing cracks on cement materials [30]. The Ring-Test consists of a steel ring with a ring cement sample poured around it. Some improvements to this test method have resulted in a few modifications to the classical circular Ring-Test (for example: elliptical Ring-Test [31-34] and dual Ring-Test [35]). A normalized version of the ring test has been proposed by AASHTO and ASTM (AASHTO [36], ASTM [37]). The standard specifications by ASTM [38] recommended a setup with metal ring internal and external radii of *152.5* and *165* mm and concrete specimens external radius and height of *203* and *150* mm.

In the Ring-Test, according to boundary conditions, drying can occur by the upper/bottom surfaces, and/or by the circumferential surfaces. So the drying direction can play a significant part in the results. Moon et al. [38] have studied using the Ring-Test the influence of specimen geometry. Their simulations results enable better selection of test specimen geometry according to moisture gradients, thickness and the stiffness of the concrete.

Analytical methods have been developed to assess tensile stresses in concrete specimen [39-41]. The basis of these methods is the equilibrium of radial pressure at the interface.

Some studies [42-46] have tried to widen the use of the Ring-Test on raw earth materials (clay, sand, etc.). However, these studies remain very limited. Using a Ring-Test, Abou Najm et al. [42] assessed the evolution of the internal stress in unsaturated soils during drying. A comparison between the measured internal stresses and existing empirical relationships using water potential curve showed a great discrepancy. They found that internal stress is not only due to the stress generated by the suction [42]. Amarisiri et al. [44] analyzed desiccation of soil using Ring-Test and compared results with numerical solutions using the discrete element method. The numerical model was proved on a kaolinite clay, then assessed with the literature results. They concluded that the Ring-Test can be a precious method to analyze fracture during drying. In order to determine the tensile strength in clay soils, Shannon et al. [45] used the restrained Ring-Test by isolating the initiation of a single crack. Four clay soils with varying shrinkage potentials were tested and analyzed.

El Hajjar et al. [47] have developed an original experimental device called DIC-CRT to study the phenomena of shrinkage and crack initiation of unsaturated soils. Their experimental measurements device combines two complementary techniques: 2D/3D-DIC and restrained Clay-Ring-Test CRT. The approach developed makes it possible to follow the strains and stresses developed in the soil during drying.

Several researches in the literature investigate the use of vegetal fibers to reinforce the soil in order to minimize shrinkage and cracking of fines soils. Fiber-reinforced soil is by definition the adding of a percentage of fibers to a soil matrix, in order to improve the mechanical behavior of the soil [48]. Tensile strength in the fibers are mobilized by shear stresses in the soil, hence give greater resistance to the soil [49, 50]. In recent years, several studies have been carried out in order to assess the effect of adding natural fibers as reinforcement of the

soil. The central role of natural fibers in today's industrial world manifested by the frequent use of the term "bio-based material" [51].

Flax fiber is a textile fiber extracted from a plant cultivated for its seeds and fibers in many regions around the world [52], including the Normandy region in France.

In order to improve the ductility of a soil-cement material, Segetin et al. [53] recommend adding flax fibers with a fiber content and length of 0.6% and 85 mm, respectively. Cheah et al. [54] developed a concept of a cheap flax fiber reinforced-earth designed as a building material. Viswanadham et al. [55] found a major impact of polypropylene fibers on delaying crack formation in clay barriers. They also showed that increasing the fiber length results in a significant delay in crack initiation. Divya et al. [56] investigated the effect of fiber content and fiber length on tensile strain and crack formation in a natural silty soil reinforced by polyester fibers. They found that fiber-reinforced soils can withstand greater strains and, consequently, higher stresses at cracking. They also found that longer fibers (60% of the sample length) provide better tensile strength and greater soil stiffness. Eid et al. [18] studied raw earth concrete based on natural silt. Their study analyzes the drying of several combinations with and without adding flax to a natural silt. Their results show that flax fibers reduces the crack ratio, defined as the cracks' area over sample's total area, by a factor of around 10. Chaduvula et al. [57] found that the addition of fibers controlled the crack width opening, the cracked area, and the propagation of cracks through the bridging action of fibers. Also, they perceive that the fibers decreased the connectivity of crack networks. Chebbi et al. [58] compared the mechanical behavior of a clay soil reinforced by vegetal fibers (Sisal fibers and Alfa fibers) with another reinforced by nylon fibers. They observed that vegetal fibers appear to be more effective than nylon fibers in improving the tensile strength of clay soils. This can be attributed to the better interfacial adhesion of the natural fibers with the reinforced soil, probably due to their greater roughness compared to the nylon fiber which has a

smoother surface. Kouta et al. [6, 10] studied the effect of natural flax fibers on plastic shrinkage and cracking at early age of earth concrete. They found that adding flax fibers reduce the total free plastic shrinkage at early age and remove the macro-cracks in sample. Furthermore, they observed a decrease in the strain localization of restrained shrinkage and the plastic shrinkage cracking.

In this paper, the DIC-CRT device [47] is used to assess the effect of flax fibers reinforcement on shrinkage and cracking of a kaolinite. Several amounts of flax fibers with orderly layout patterns have been studied using this DIC-CRT device. The aim of this work is to connect the two measurement techniques, based on Digital Image Correlation (DIC) and Clay-Ring-Test (CRT), in order to assess crack initiation and propagation in reinforced soils during desiccation. These two techniques can reveal the impact of reinforcement on the level and the kinetic of crack opening. The relationship between suction and strain evolution is studied in order to highlight the influence of suction on clay shrinkage that lead to cracking. Furthermore, a definition of a relevant parameter to quantify crack intensity in materials is proposed.

## **II – MATERIALS AND METHODS**

Shrinkage and cracking of a clay material due to desiccation was investigated using three experimental devices: DIC coupled with CRT for strain measurement and tensiometers for suction measurement.

### **II.1 - Materials**

The clay material used in this work is a yellow kaolin called P300. Table 1 presents its geotechnical properties.

Table 1: Geotechnical properties of the kaolin P300 [59].

Properties	Symbol	Value
Grain size distribution	< 80 $\mu\text{m}$ (%)	100
	< 2 $\mu\text{m}$ (%)	60
	$d_{50}$ ( $\mu\text{m}$ )	1.5
Plasticity	LL (%)	40
	PL (%)	21
	PI (%)	19
Specific Gravity	Gs	2.65

According to XRD and SEM image analysis of this kaolin P300 [28, 59], this clay contains 95% of kaolinite and small percentages of illite and quartz. The shape of its particles is in rigid hexagonal plates with size of 1 to 2  $\mu\text{m}$ . The SWRC (Soil Water Retention Curve) of the kaolin P300 studied by Fleureau et al. [60] is presented in Figure 1.

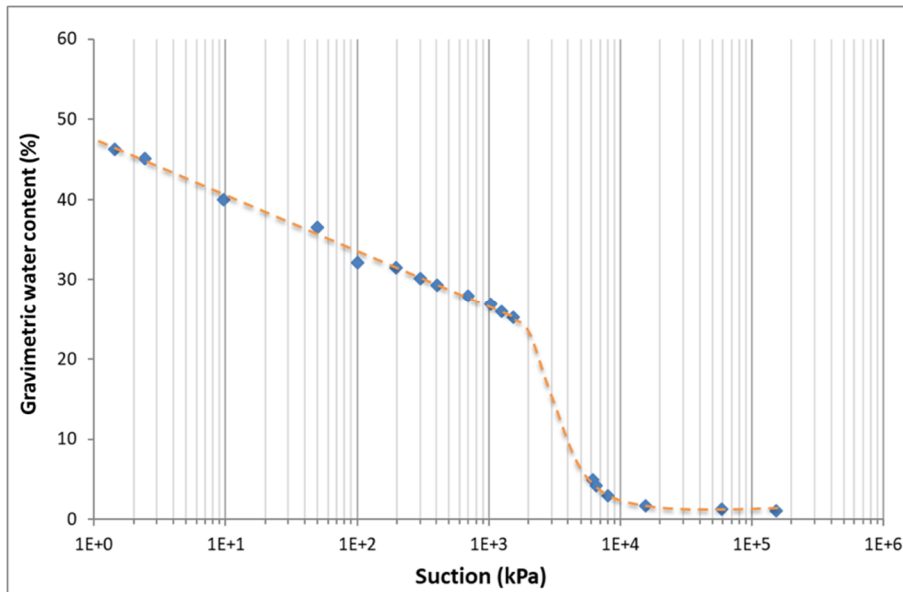


Figure 1: SWRC of the kaolin P300 [60].

A mixed kaolinite and water to a water content of 60% ( $w = 60\%$ ) is prepared in order to get a saturated slurry material. Before being poured into the mold, kaolinite slurry has been kept for 24 hours in a closed container, so that its water content being homogeneous. In order to minimize the friction between the clay material and the mold, the bottom of the mold was covered with a Teflon sheet of 1 mm thick with a 0.08 friction coefficient.

The flax fibers used in this study were extracted locally, in the Normandy region (France). These fibers are in the form of a continuous thread with a density of  $1400 \text{ kg/m}^3$  and thickness of 1.2 mm. Tensile properties of flax fibers are essential when using it as a reinforcement. The tensile behavior of a flax fiber is not constant and depends on the selected specimen, even if the fibers are cultivated in the same location, and tested in the same way [60]. Table 2 list mechanical properties of flax fibers used in this study (absolute density  $\rho$ , Young modulus  $E$ , ultimate strain  $\epsilon_u$  and ultimate stress  $\sigma_u$ ).

*Table 2: Flax fibers properties [18].*

$\rho \text{ (kg/m}^3\text{)}$	$E \text{ (GPa)}$	$\epsilon_u \text{ (\%)}$	$\sigma_u \text{ (MPa)}$
1400	40 - 85	2.4 - 3.3	800 - 2000

## II.2 - DIC methods

DIC basic principle is to match two speckled patterns between reference and current images. The software compares the grayscale distributions in the corresponding pixel patterns of the two images to obtain the field of displacement and the compute the corresponding strains. A grid of measuring points is formed by dividing image into subsets. Parameters of DIC method used in this study are given in Table 3.

*Table 3: Images processing parameters.*

<b>Parameter</b>	<b>Value</b>
Image resolution	3150 x 3150 pixels
field of view	200 x 200 mm
speckle size	0.16 mm
displacement precision	0.1 mm
step size	5 pixels
subset size	21 x 21 pixels

For more details, all DIC processing parameters and calibration are given in El Hajjar et al. [47], according to iDIC good-practices guidelines [61].

A cold lamp bulb was used to homogenize the color distribution, and an opaque black curtain was added all around the used setup. Relative humidity  $RH = 18 \% (\pm 2\%)$  and temperature  $T = 22^{\circ}\text{C}$  were controlled in the experimental tests using hygrothermal controlled room. A black and white PVC powder composed of particles with a diameter of about  $160 \mu\text{m}$ , was used as a speckled pattern over the specimen to enable correct pixel detection. The DIC analysis was carried out with commercial software package.

### **II.3 - Clay-Ring-Test (CRT)**

The Clay-Ring-Test used in this study was made of aluminum (Aluminum 2017a-AU4G). It has a cylindrical ring shape with 25 mm internal radius, 30 mm external radius (i.e. 5 mm thickness) and 30 mm height. The soil was poured around the external face of the ring to a 100 mm external radius (i.e. 70 mm of soil thickness). Specimen height was selected according to several preliminary tests on clayey materials [47]. Four gages measuring the micro strains produced by the applied pressure to the metal ring were added at half-height of its inner face. Three tensiometers (T1, T2 and T3), with a measuring range between 0 and 90 kPa, were included in the device to measure suction evolution during the drying process. The CRT device and the sample were set up on a balance having a precision of 0.05 g, allowing to record the evolution of the sample weight throughout the drying process and to determine its actual water content. A descriptive scheme of the DIC-CRT device with the tensiometer sensors (presented in the next paragraph) is shown in Fig.2.

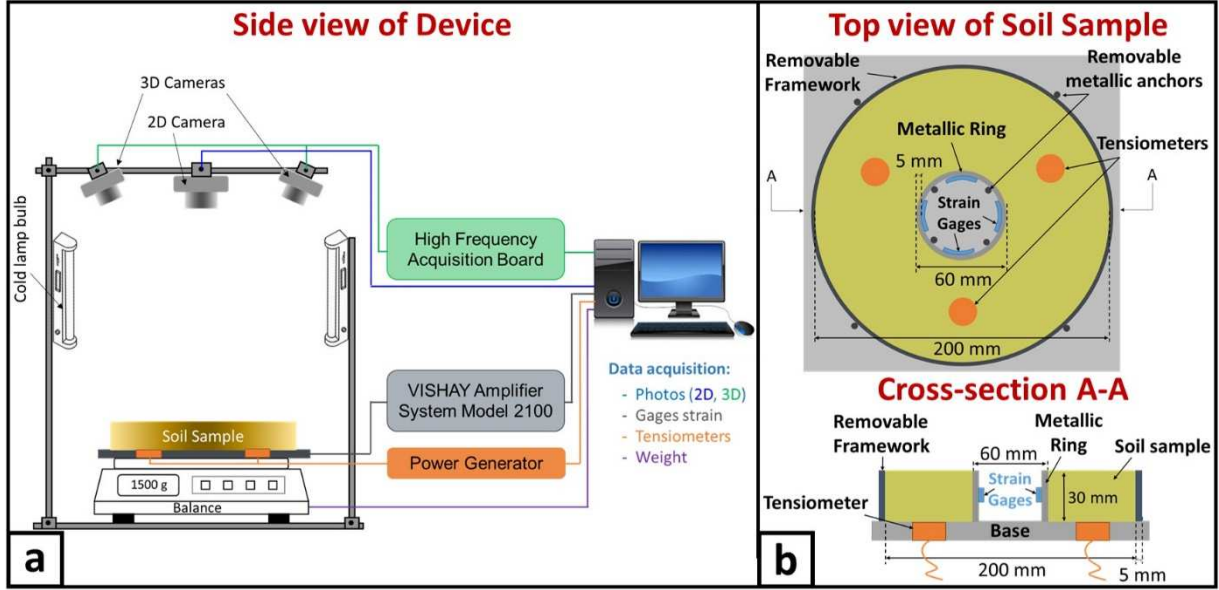


Figure 2: Descriptive scheme of the experimental device: (a) Device's side view with data acquisition systems, (b) Soil Sample's Top view with section view.

Using the strains measured by the gages on the inner circumference of the aluminum ring, the stresses applied by the soil can be deduced [47]. Due to desiccation, the soil specimen is subjected to suction; the latter pressure was considered to act at the inner surface of the soil in contact with the aluminum ring. In turn, the ring is subjected at its outer surface to an opposite and equal pressure.

The soil is submitted in-plane to circumferential tensile stress ( $\sigma_{\theta\theta}$ ), radial compressive stress ( $\sigma_{rr}$ ) as well as shear stress ( $\sigma_{r\theta}$ ). Figure 3 shows an element of the soil ring with all in-plane stresses represented in polar coordinate system, where  $r$  and  $\theta$  are the radial and angular coordinates. As consequence, the soil deforms following strain tensor  $\epsilon_{rr}$ ,  $\epsilon_{\theta\theta}$  and  $\gamma_{r\theta}$  defined as radial strain, circumferential strain and angular strain, respectively. In this paper,  $\epsilon_{\theta\theta}$  is called circumferential S-strain in soil and circumferential G-strain in metal ring.

The maximum tensile stress ( $\sigma_{\theta\theta}$ ) that develops in soil specimen can be obtained using the following equation:

$$\sigma_{\theta\theta} = -\epsilon_{Alu}|_{(r=R_{IR})} E_{Alu} \frac{R_{OR}^2 - R_{IR}^2}{2 R_{OR}^2} \frac{R_{OS}^2 + R_{OR}^2}{R_{OS}^2 - R_{OR}^2}$$

Where,  $\epsilon_{\text{Alu}}|_{(r=R_{\text{IR}})}$  is measured strain at inner radius of aluminum ring,  $E_{\text{Alu}}$  is Young's modulus of restraining ring,  $R_{\text{IR}}$  and  $R_{\text{OR}}$  are inner and outer radius of aluminum ring, respectively, and  $R_{\text{OS}}$  is outer radius of soil specimen.

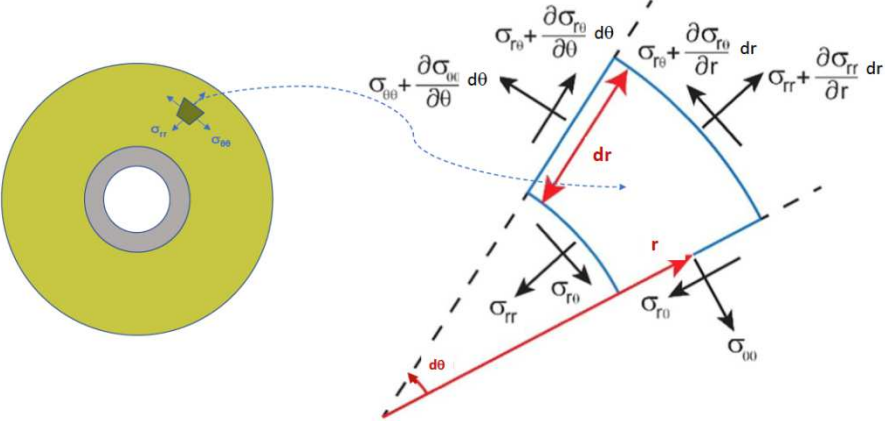


Figure 3: An element of the soil ring with all in-plane stresses in polar coordinate system.

**II.4 - Suction measurement by tensiometry**

The suction, negative pore-water pressure, developed in soil was measured using a tensiometric testing method. It consists of a saturated ceramic of 12 mm diameter related to a de-aired water tank having a relatively small volume. The water pressure was measured using an absolute pressure sensor placed below the water tank (Figure 4). The sensor is a pressure transmitter Type A-10 that measures an absolute pressure varying between 0 and 1600 kPa (with respect to void), through an output signal ranging from 0 to 10 VDC, with an uncertainty of about 2%.

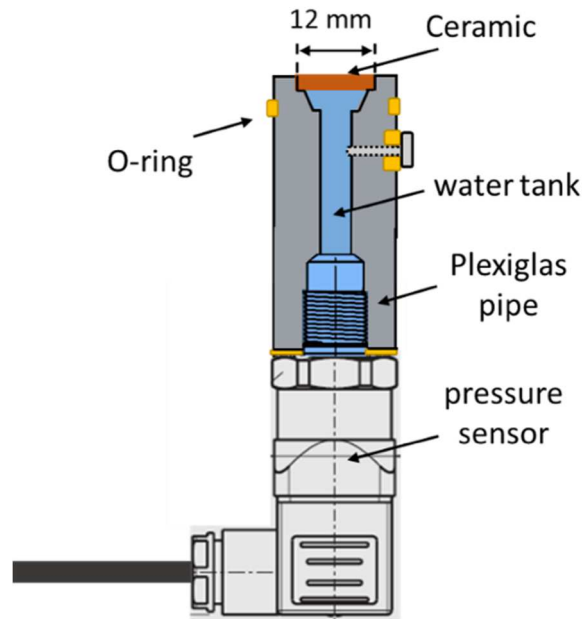


Figure 4: Descriptive Scheme of the developed tensiometer.

In order to assess the response time of the ceramic, suction measurements were performed on an unsaturated clay sample. Test results are presented in Figure 5. At the beginning of the test (before point A), the sensor was subjected to atmospheric pressure. Therefore, an absolute pressure of 102 kPa was measured. At point A, the tensiometer got into contact with the clay sample. The pressure's value began to decrease down to an absolute pressure of about 10 kPa, reached within a response time of 10 minutes. This pressure corresponds to a measured suction of 90 kPa. It remained constant until the end of the experiment. Hence, this value of 90 kPa represents the maximum suction able to be measured by this sensor.

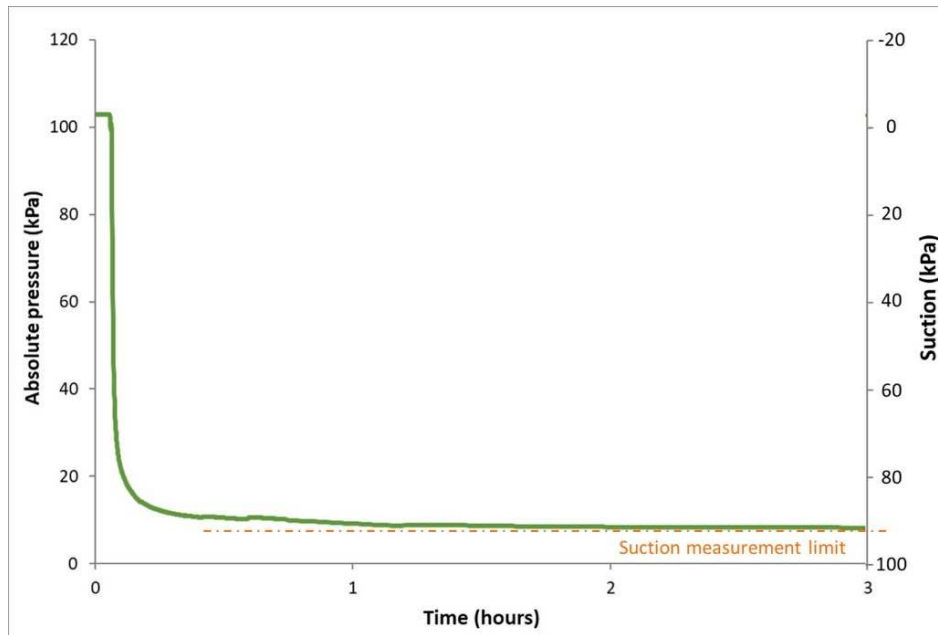


Figure 5: Tensiometer measurements on a dry clay sample.

## II.5 – Shrinkage testing protocol

Seven tests were carried out to evaluate the impact of adding flax fibers to clayey soil. Two control samples K1 and K2 do not contain any flax fibers and five samples, KF3 to KF7, with varying flax fibers percentages and orientations. List of samples is presented in Table 4; photos shown were taken after pouring the kaolinite to half of its thickness and putting flax fibers in some of the specimens as shown in Figure 6(S2). In samples KF3 and KF4, flax fibers were embedded in the circumferential direction only, over half the cross-section and over the entire cross-section, respectively. In samples KF5, KF6 and KF7, flax fibers were embedded in both circumferential and radial directions, in order to withstand both major and minor principal strains. In addition, fibers in sample KF6 presented loops spaced at 1 cm, designed to improve adherence between fibers and clay paste. In sample KF7, fibers were enrolled together to 2.4 mm of diameter (previously 1.2 mm) to improve their strength. Noting that the proportion of fibers shown in Table 4 represents the fiber area proportion at mid-height of the sample, and not the volume proportion. For instance, for a fiber area proportion of 30% (KF7 sample), we obtain a fiber mass content of 1%. For these drying

tests, several preliminary tests were carried out previously for each case in order to check the tests reproducibility. Globally, these preliminary tests had shown a good agreement between the amount and the pattern of reinforcement and the observed results. In this paper, we have focused only on showing one result from these several tests, that is consistent with the general observed tendency.

Table 4: Description of the test samples.

Sample	Description	Fibers amount	Photo
K1	Kaolinite without flax fibers	0 %	
K2			
KF3	Flax fibers in circumferential direction over half cross-section	5 %	
KF4	Flax fibers in circumferential direction over entire cross-section	10 %	
KF5	Flax fibers in circumferential and radial directions	15 %	
KF6	Flax fibers in circumferential and radial directions with loops 	20 %	
KF7	Flax fibers having a <b>double diameter</b> in circumferential and radial directions 	30 %	

Figure 6 presents the different steps for sample preparation; KF7 is taken as an example. An external removable formwork of PVC was used during preparation to contain the clay. To keep the aluminum ring and external formwork fixed during clay pouring, metal anchors were used as shown in Figure 2 and Figure 6(S1). After pouring 1.5 cm layer of clay, flax fibers

were embedded in circumferential and radial directions at mid-height of the sample (stage S2). Fibers rows were spaced 1 cm in both circumferential and radial directions. A second layer of clay, 1.5 cm thick, was then poured over the fibers (stage S3). After pouring the clay, metal anchors and formwork were removed to make the displacement of the aluminum ring and sample free. To prevent the material flowing due to its very high initial water content, its outer circumference was retained by a paper tape. A speckle pattern made of PVC particles was scattered all over the clay. This speckle pattern allows DIC software to detect the pixels' displacement on the upper surface of the sample (stage S4).

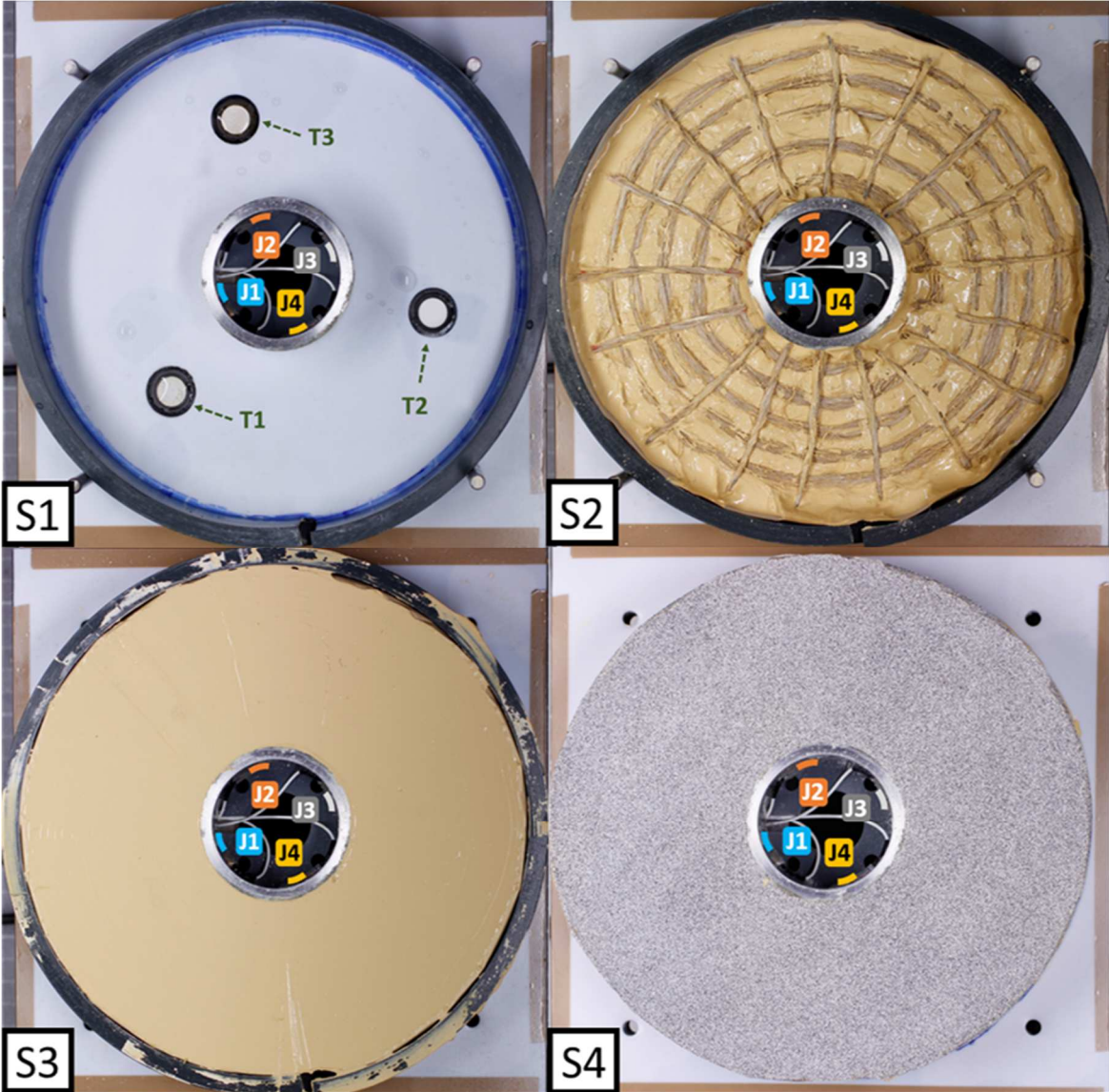


Figure 6: Preparation stages. Example of sample KF7.

### III – RESULTS AND DISCUSSION

#### III.1 – Water content and suction evolution

Figure 7 shows water content evolution during drying. During the initial drying phase, water evaporation was constant with a drying kinetic ranging between -8%/day and -8.5%/day. Beyond a water content equal to 5%, the drying kinetic decreased and the water content tended towards a residual water content around 1%. End of the test was achieved once the water content of the sample became stable and reached a horizontal plateau, after 10 days of drying time. The first crack appeared at water contents ranging randomly from 24.5%-26.5%, corresponding to suctions ranging from 1200-1800 kPa. It can be noted that water content variation and first crack initiation were similar for the seven samples.

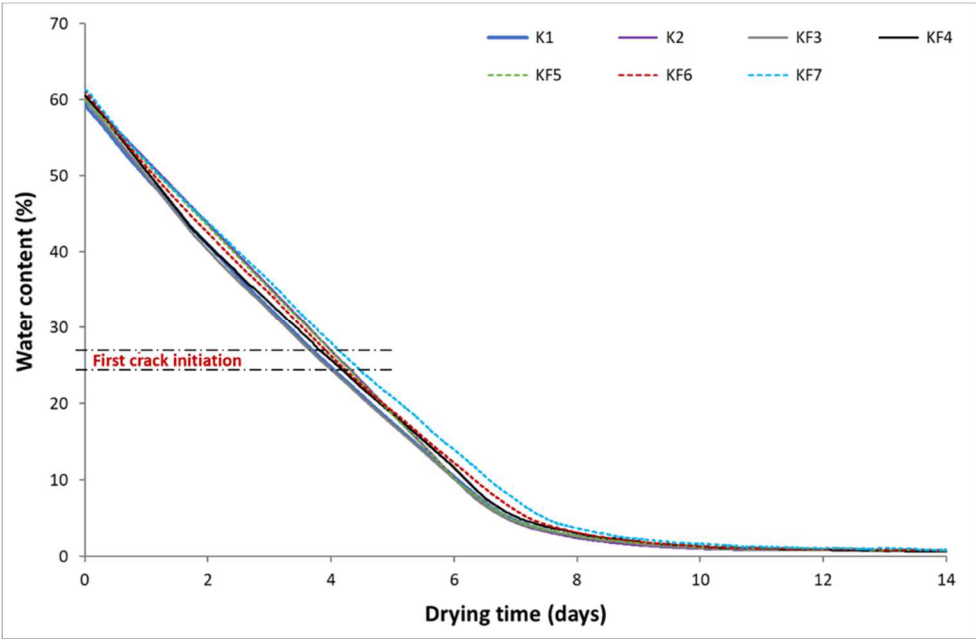


Figure 7: Water content's evolution during drying for the seven samples.

Figure 8 presents the variation of the measured suction by the CRT tensiometers during drying as well as the suction deduced from the SWRC [60]. The latter is a function of the water content which is, in turn, function of drying. SWRC ranged between 0 and 150 MPa, while CRT tensiometers had a measurements range between 0 and 90 kPa. Within the

tensiometers measuring range, good agreement can be seen between the suction measured by CRT tensiometers and that deduced from SWRC. Also, the three CRT tensiometers showed very close suction variations despite their different locations below the sample.

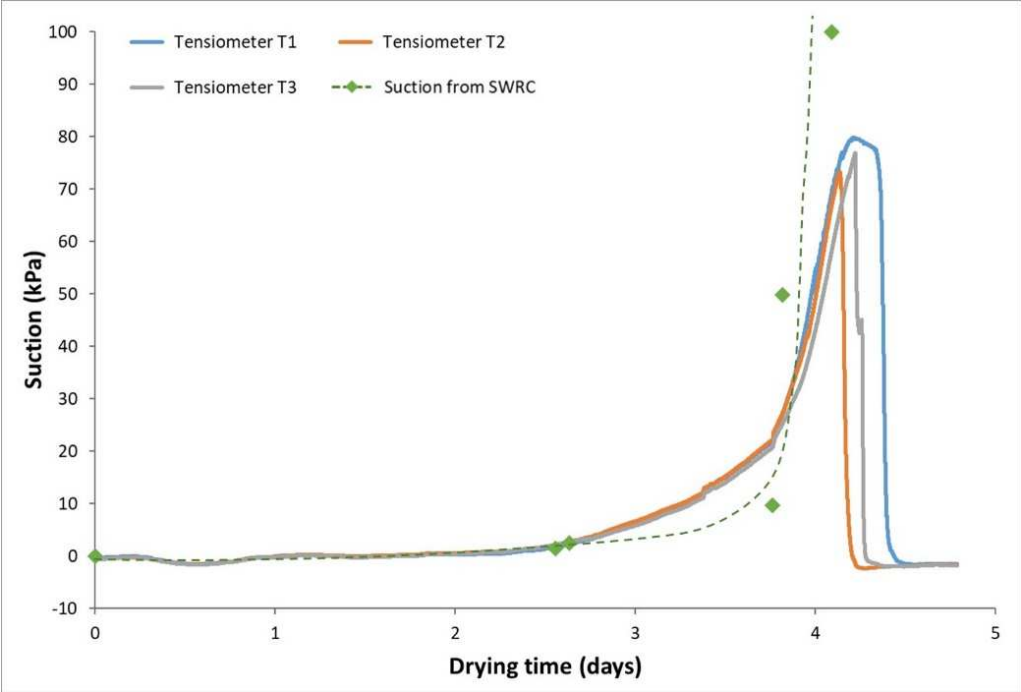


Figure 8: Suction’s variation with drying: CRT tensiometers measurements and SWRC.

**III.2 – CRT strains**

Figure 9 and Figure 10 show the circumferential strain variation in the aluminum ring (G-Strain) as a function of drying time that present four phases.

Figure 9 presents the phase A, a preliminary step that consisted in pouring the clay slurry in the device mold. A negative strain value of about -10  $\mu\text{m}/\text{m}$  was observed during the first 10 minutes. Note that a negative circumferential strain value means that the clay undergoes a compression against the metal ring. This strain corresponded to the gages response to clay pouring process, applied to the outer circumference of the ring.

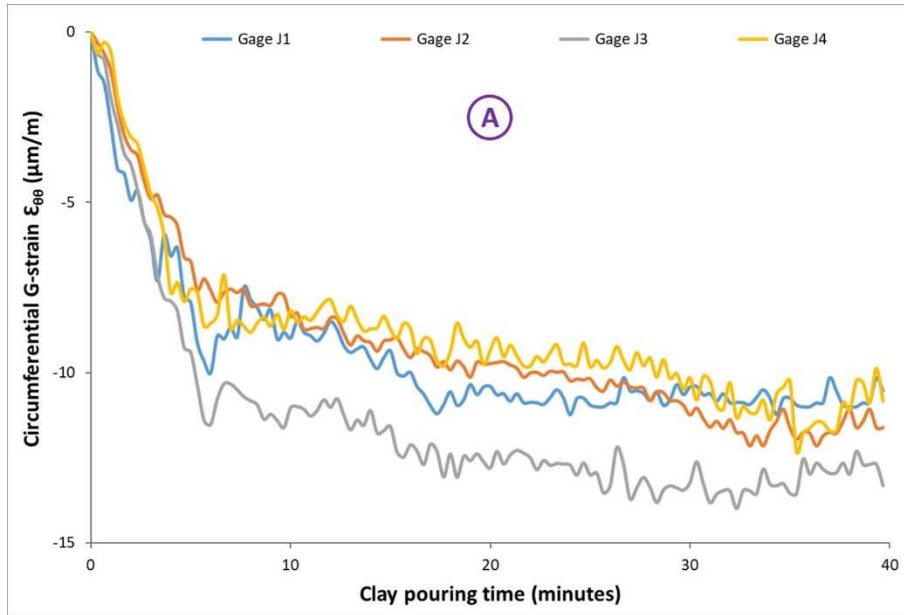


Figure 9: Evolution of circumferential strains in aluminum ring during clay pouring.

Figure 10 presents circumferential strains variation in the aluminum ring during drying after phase A. During phase B (0 to 2.5 days), strain gages show a reset of the circumferential strain that increased and became positive. This is due to metal ring decompression occurred as a result of a slight expansion of the clay slurry after removing the formwork, in addition to a likely beginning of clay shrinkage. In phase C, the strain decreased and featured two subphases. During phase C1, the shrinkage increased and the metal ring quickly deformed with a slope equal to  $-5 \mu\text{m/m/day}$  until a drying time of 3.5 days. Then, strain decreasing rate accelerated to  $-20 \mu\text{m/m/day}$  during phase C2 until cracking occurred for a maximal circumferential strain of about  $-20 \mu\text{m/m}$ . After cracking, the ring deformation inverted to an opposite direction and increased with a slope equal to  $5 \mu\text{m/m/day}$  (phase D). This may be attributed to the cracks' formation which relaxed the ring compression. The relaxation of the stresses in the metal ring prevents the follow-up of the crack propagation by G-strain evolution.

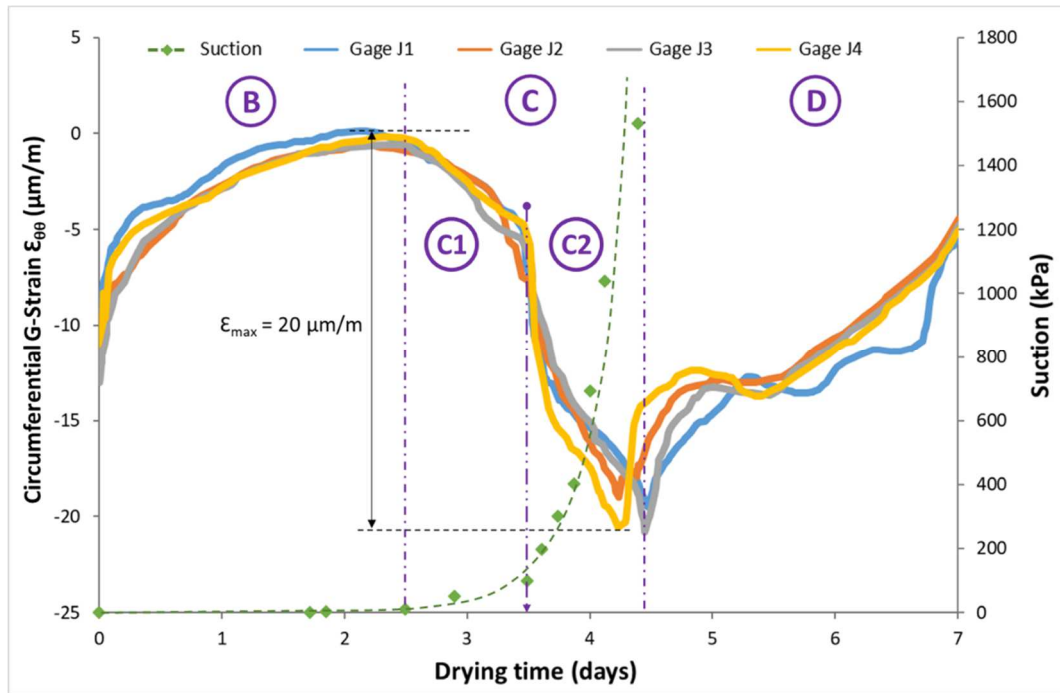


Figure 10: Circumferential strain's variation during drying. Comparison with suction evolution.

Evolution of suction deduced from SWRC [60] is also plotted in Figure 10. A good agreement is noticed between suction increase and strain decrease in phase C1 between 2.5 days and 3.5 days of drying time, as well as in phase C2 until cracking occurred at 4.3 days for a suction of about 1500 kPa. This correlation between clay suction and circumferential strain in metal ring reveals the direct influence of suction on clay shrinkage. This statement may be substantial for researchers in the study of the origin of shrinkage strains leading to clay cracking. Note that suction represents internal stresses developed in the material during drying.

### III.3 – Shrinkage and cracking analysis

As the drying process progressed, sample shrunk radially and some cracks appeared in this direction starting from the inner circumference of the sample (Figure 11). The blue circle represents the sample boundary in initial state. A shrinkage of sample radius of about 1 cm ( $\pm 0.15$  cm) was observed. Cracks shown in the sample are labeled following the chronological order of formation, based on DIC analysis. Sample failure corresponded to crack growth towards outer circumference of the sample (Crack Cr4), resulting in a reset of the ring

compression (end of phase D in Figure 10). Order of cracks initiation showed that the first crack is not necessarily the one that leads to sample failure.

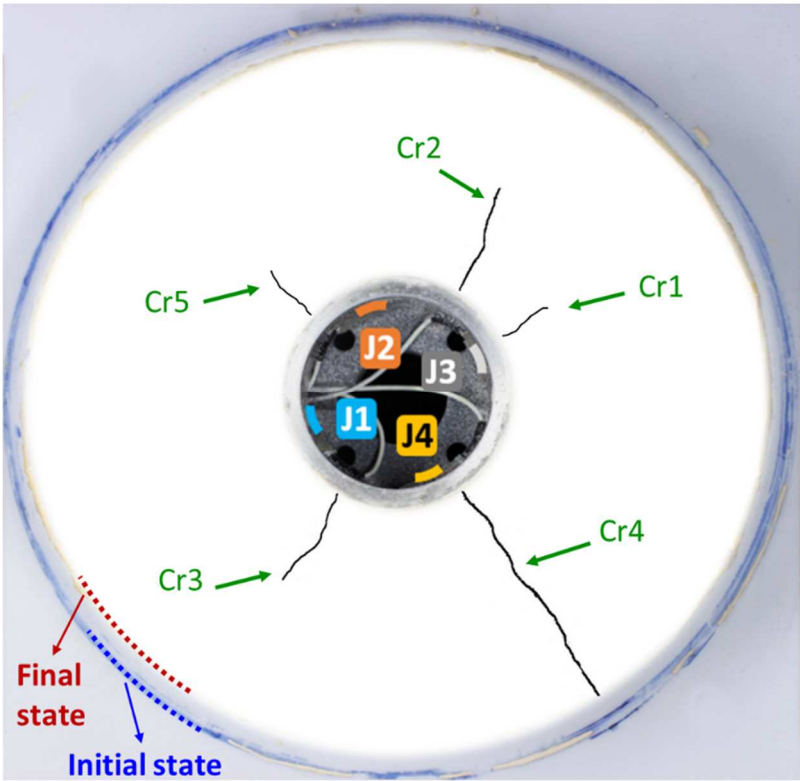


Figure 11: Cracks pattern at the end of the drying process. Example of KF7 sample.

At the end of the drying process, when the sample water content reached its residual value, the global shrinkage ratio was computed. It is defined as the difference between the initial and final areas of the specimen over its initial area. The global shrinkage ratio of the different samples is presented in Figure 12. It ranges from 23%-27%, with a mean value of about 25%, whatever the added fibers. Flax fibers do not show any significant influence on global shrinkage ratio. This is may be due to the mean stiffness (strain modulus) of samples which are not affected by the added fibers. Note that the fiber mass content is negligible in the studied samples (less than 1%), so that it will probably not have a significant effect on its mean stiffness [10]. Crack ratio was also calculated. It is defined as the cracks area over the sample final area. Its variation was plotted on the same graph (Figure 12). For samples without flax fibers (samples K1 and K2), the crack ratio was around 0.8%. This ratio

decreased steeply in the samples with added fibers regardless of their placement. For sample KF7 with 30% added fibers, crack ratio reached a minimum value of about 0.1%. The significant decrease of crack ratio, by a factor of about 8, as a function of fibers amount in samples highlighted the impact of soil reinforcement by flax fibers on the level of crack opening. The reason of crack ratio decrease may be that reinforcement takes part of the mechanical solicitation applied to clay matrix, through soil/fibers friction. This observation matches with Kouta's and Eid's results that adding flax fibers remove the macro-cracks in sample [6, 18].

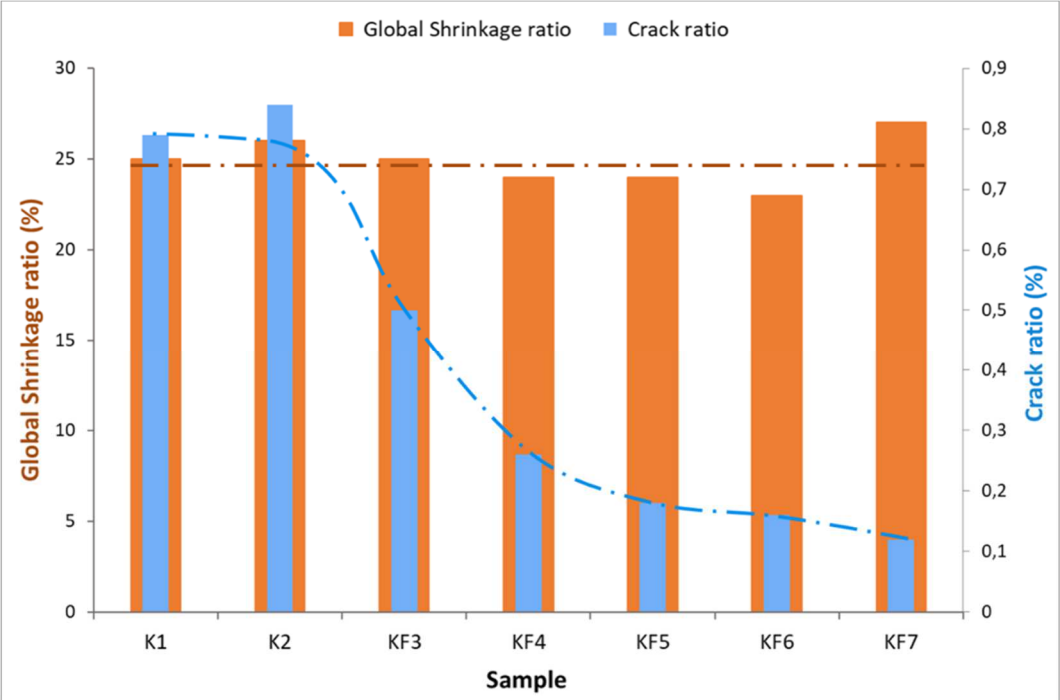


Figure 12 : Global shrinkage ratio and crack ratio at the drying process end.

**III.4 – DIC strains**

El Hajjar et al. [47] have shown that circumferential strain ( $\epsilon_{\theta\theta}$ ) developed in the soil corresponds to the major principal strain leading to the crack formation and is maximal near the metal ring.

In this study, using DIC technique, the variation of the circumferential strain near the metal ring, at a radius of 35 mm, was plotted in Figure 13. This radius represents the nearest point to

the metal/soil interface where DIC analysis is possible. Note that for vertical drying, the evolution of the located S-strain shows that the cracks start from the inner diameter of the ring sample and propagate radially outwards [47]. Samples without flax fibers (K1 and K2) showed very high peaks with circumferential strain values reaching about 40%. On the other hand, sample KF3 that contains flax fibers embedded only over the half of its cross-section showed lower peaks ranging from 5%-20%. In the samples containing flax fibers embedded over the entire cross-section, the circumferential strains were comprised between 0% and 2%. This result highlights the impact of soil reinforcement by flax fibers on the major principal strains. Crack intensity was defined as the maximum major principal strain leading to cracking at the interface with the metal ring (peaks on Figure 14). Reinforcement with flax fibers made soil cracking less prejudicial by reducing its intensity (Figure 14).

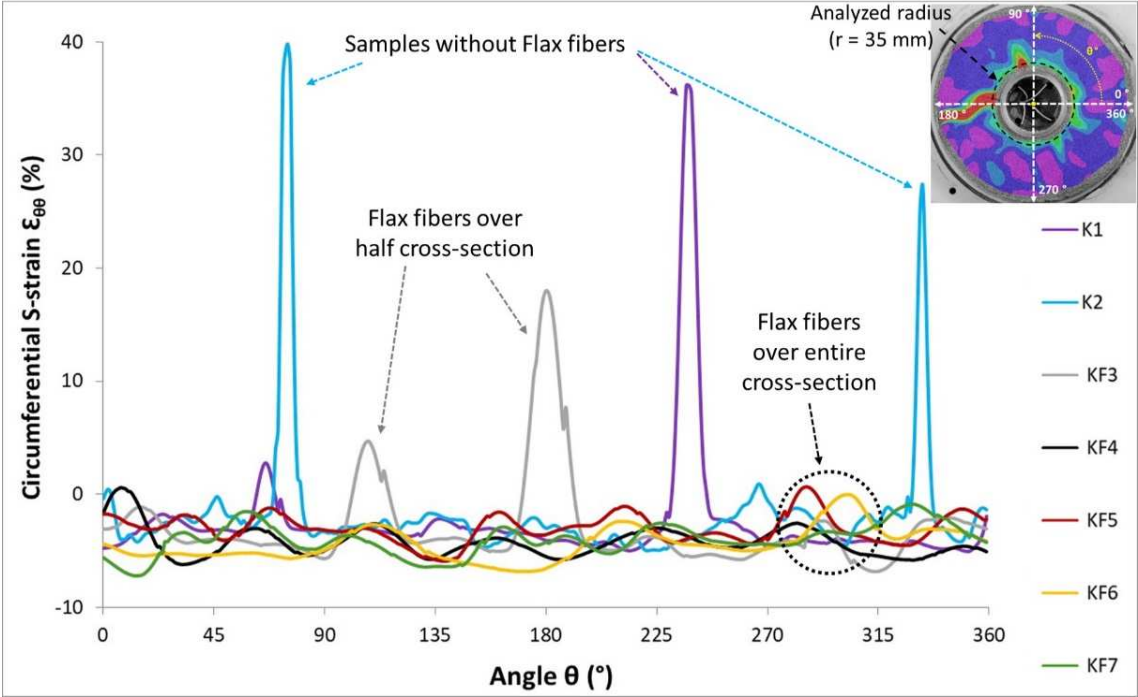


Figure 13 : Circumferential strain variation at the interface with the metal ring function of the angle  $\theta$  of soil ring contour.

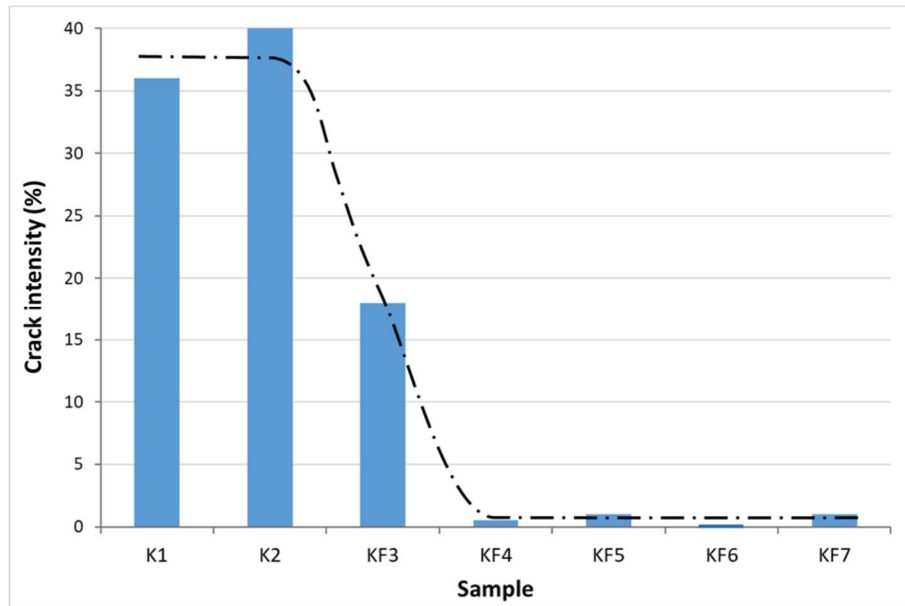


Figure 14 : Crack intensity variation at the interface with the metal ring.

### III.5 – DIC vs CRT strains

Circumferential strain variation as a function of water content is plotted in Figure 15, where the results obtained from the two methods - DIC (photos a) and CRT (photo b) - for sample K1 without flax fibers are compared. The maximum circumferential S-strain value obtained from DIC is shown in Figure 15(a). It decreased slightly at the beginning of the drying process until reaching a strain of -1.2% when the sample cracked at a water content of 25.5%. After cracking, circumferential strain increased quickly with crack opening until it became stable at a maximal circumferential strain of 36% that corresponded to a water content of about 22%. The DIC slope was defined as the slope of the maximum circumferential strain value increase versus the water content decrease, in the soil sample at a radius of 35 mm during soil cracking.

Figure 15(b) shows CRT circumferential G-strain variation as a function of water content obtained from gage J4. It decreased at the beginning of the drying process until the sample cracked at a water content of 25.5%. After cracking, an abrupt change was observed in the circumferential strain of the metal ring, then it increased slightly until it became stable at a circumferential strain of about 5  $\mu\text{m}/\text{m}$ , corresponding to a water content of about 22%. The

CRT slope was defined as the slope of the circumferential strain increase versus the water content decrease, in the inner circumference of the metal ring during soil cracking. The slope of the abrupt changes after cracking was computed for the four strain gages of the metal ring. CRT slope corresponds to the maximum slope for each of them.

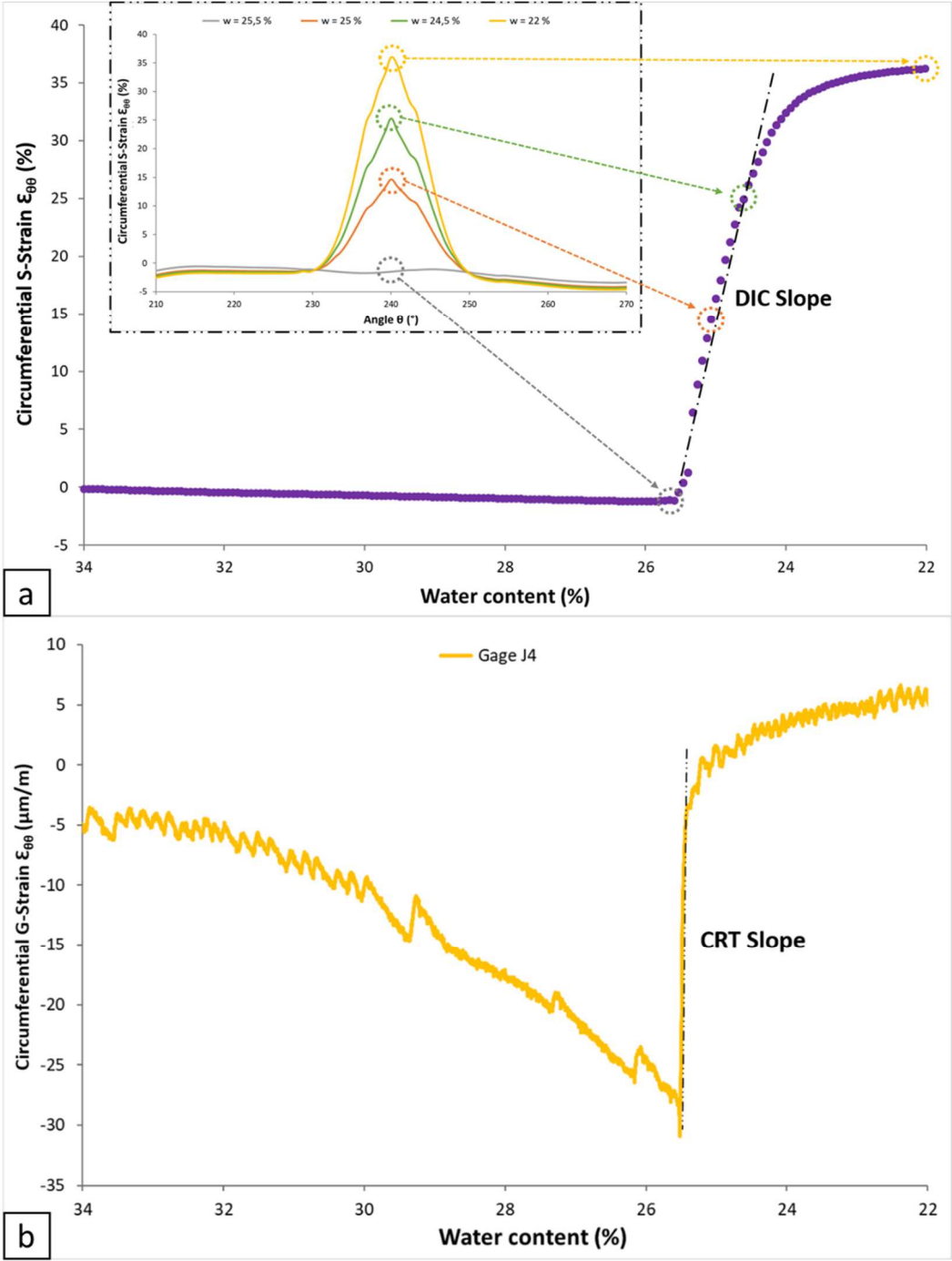


Figure 15 : (a) Evolution of maximal circumferential strain (from DIC) in sample K1 as a function of water content  
 (b) Evolution of gage J4 circumferential strain (from CRT) in sample K1 as a function of water content

Figure 16 presents a comparison between DIC slope and CRT slope for all samples. A good agreement was observed between the two slopes obtained from the two different methods, DIC and CRT. Samples K1 and K2, with no added flax fibers, showed a DIC slope of about 22 %/‰ and a CRT slope of about  $130 \cdot 10^{-4}$  %/‰. The two slopes decreased with the flax fibers amount and reached 1 %/‰ for DIC slope and  $3 \cdot 10^{-4}$  %/‰ for CRT slope, for samples KF6 and KF7. The significant decrease of DIC and CRT slopes, by a factor of about 20, highlights again the impact of soil reinforcement by flax fibers on the kinetic of crack opening. Also, the presence of loops in sample KF6 and intertwined fibers in sample KF7, which aimed to enhance soil/fibers friction, seemed to reduce DIC and CRT slopes. The reason was that reinforcement seeks to slow down cracks opening through soil/fibers friction. Therefore, CRT slope and/or DIC slope represent a relevant parameter to describe the effect of flax fibers on the kinetic of crack opening. This statement seems to be similar to Chaduvula's observation that the addition of fibers controlled the propagation of cracks through the bridging action of polyester fibers [57]. Furthermore, we did not observe a significant impact of the fiber orientation on the deformation and cracking of the clay sample during drying, as can be seen when comparing KF4 and KF5 samples. This is because in this axisymmetric sample the crack initiates perpendicular to the circumferential direction. This is due to the reason that the tensile strains which lead to material failure are concentrated in this circumferential direction [47].

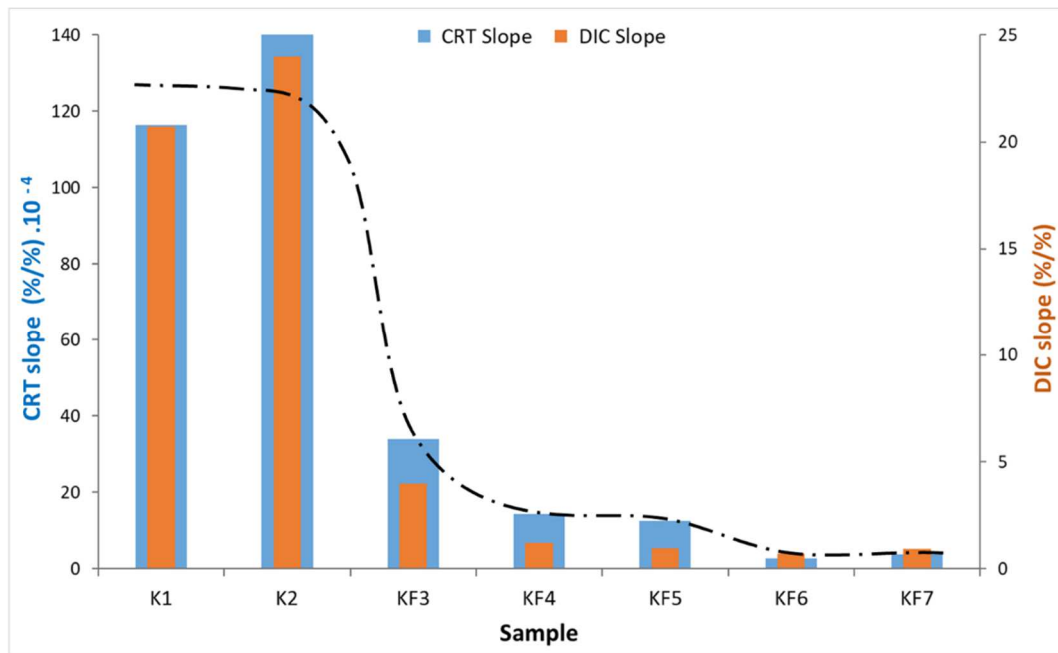


Figure 16 : CRT slope and DIC slope for all samples

#### IV – CONCLUSION

An experimental study of cracking of fine clayey soils by desiccation was carried out using a coupled DIC-CRT device. Several amounts of flax fibers as well as different patterns of fibers layout have been investigated. Suction measurements in samples were performed during desiccation using tensiometers. A good agreement was noticed between suction increase in clay and strains leading to cracking, which highlighted the direct influence of suction on clay shrinkage and cracking. This is because that suction is a main factor causing desiccation shrinkage in unsaturated soils.

For a drying kinetic of about 8 %/day, soil reinforcement by flax fibers led to the following conclusions:

- 1- CRT analysis shows that there is no significant impact of added flax fibers on crack initiation in soil, evidenced by the water contents at which strains in metal ring begin to relax.
- 2- Soil reinforcement by flax fibers does not affect global shrinkage, but it has a significant influence on crack ratio which decreases by a factor of about 8. This highlights the impact of

soil reinforcement by flax fibers on the level of crack opening. This observation matches with Kouta's and Eid's results that adding flax fibers remove the macro-cracks in sample [6, 18].

3- DIC analysis shows that flax fibers reinforcement reduces significantly the evolution of the major principal strain leading to clay cracking, in opening mode, i.e. by extension. This observation reveals that reinforcement with flax fibers made soil cracking less prejudicial by reducing its intensity.

4- DIC and CRT slopes, representing maximal strains variation during material cracking, show a good agreement between these two techniques, and allow to better analyze crack propagation and opening. These slopes decrease significantly, by a factor of about 20 in clay samples reinforced by flax fibers due to soil/fiber friction, which highlights the impact of soil reinforcement by flax fibers on the kinetic of crack opening. This statement seems to be similar to Chaduvula's observation that the addition of fibers controlled the propagation of cracks through the bridging action of polyester fibers [57].

### **Acknowledgments**

This work was supported by region of Normandy (France).

## REFERENCES

- [1] Pacheco-Torgal, F., & Jalali, S. (2012). Earth construction: Lessons from the past for future eco-efficient construction. *Construction and building materials*, 29, 512-519.
- [2] Boivin, P., Garnier, P., Vauclin, M. (2006). Modeling the soil shrinkage and water retention curves with the same equations. *Soil Science Society of America Journal* 70 (4), 1082–1093.
- [3] Zornberg, J.G., Kuhn, J., and Wright, S. (2007). Determination of Field Suction Values, Hydraulic Properties and Shear Strength in High PI Clays. Research Rep. 0-5202-1, Center for Transportation Research, Univ. of Texas at Austin.
- [4] Laborel-Preneron, A., Aubert, J. E., Magniont, C., Tribout, C., & Bertron, A. (2016). Plant aggregates and fibers in earth construction materials: A review. *Construction and Building Materials*, 111, 719-734.
- [5] Chauhan, P., El Hajjar, A., Prime, N., Plé, O. (2019). Unsaturated behavior of rammed earth: Experimentation towards numerical modelling. *Construction and Building Materials*, 227, 116646.
- [6] Kouta, N., Saliba, J., & Saiyouri, N. (2020). Effect of flax fibers on early age shrinkage and cracking of earth concrete. *Construction and Building Materials*, 254, 119315. <https://doi.org/10.1016/j.conbuildmat.2020.119315>
- [7] Kodikara, J. K., Barbour, S. L. Fredlund, D. G. (2000). Desiccation cracking of soil layers. *Proceedings of the Asian conference on unsaturated soils: From theory to practice*, Singapore, pp. 693 – 698.
- [8] Nahlawi, H. and J. K. Kodikara (2006). "Laboratory experiments on desiccation cracking of thin soil layers." *Geotechnical & Geological Engineering* 24(6): 1641-1664.
- [9] Peron, H., Laloui, L., Hueckel, T., Hu, L. (2009). Desiccation cracking of soils. *Eur. J. Environ. Civ. Eng.* 13, 869–888.
- [10] Kouta, N., Saliba, J., & Saiyouri, N. (2020). Fracture behavior of flax fibers reinforced earth concrete. *Engineering Fracture Mechanics*, 107378. <https://doi.org/10.1016/j.engfracmech.2020.107378>
- [11] Péron, H., Herchel, T., Laloui, L., Hu, L.B. (2009). Fundamentals of desiccation cracking of fine-grained soils: experimental characterization and mechanisms identification. *Canadian Geotechnical Journal* 46, 1177–1201.
- [12] Wei, X., Bicalho, K. V., El Hajjar, A., Taibi, S., Hattab, M., & Fleureau, J. M. (2020). Experimental Techniques for the Study of the Cracking Mechanisms in Drying Clays. *Geotechnical Testing Journal*, 44(2). <https://doi.org/10.1520/GTJ20190430>
- [13] Tang, C.S., Cui, Y.J., Tang, A.M., Shi, B. (2010). Experimental evidence on the temperature dependence of desiccation cracking behavior of clayey soils. *Engineering Geology* 114, 261–266.

- [14] Hedan, S., Valle, V., & Cosenza, P. (2020). Subpixel precision of crack lip movements by Heaviside-based digital image correlation for a mixed-mode fracture. *Strain*, e12346.
- [15] Tang, C. S., Zhu, C., Leng, T., Shi, B., Cheng, Q., & Zeng, H. (2019). Three-dimensional characterization of desiccation cracking behavior of compacted clayey soil using X-ray computed tomography. *Engineering Geology*, 255, 1-10.
- [16] Hedan, S., Fauchille, A. L., Valle, V., Cabrera, J., & Cosenza, P. (2014). One-year monitoring of desiccation cracks in Tournemire argillite using digital image correlation. *International Journal of Rock Mechanics and Mining Sciences*, 68, 22-35.
- [17] Wei, X., Hattab, M., Bompard, P., & Fleureau, J. M. (2016). Highlighting some mechanisms of crack formation and propagation in clays on drying path. *Géotechnique*, 66(4), 287-300. <https://doi.org/10.1680/jgeot.14.P.227>
- [18] Eid J., Taibi S., Fleureau J.M. and Hattab M. (2015). Drying, cracks and shrinkage evolution of a natural silt intended for a new earth building material. Impact of reinforcement. *Construction and Building Materials*, 86, 120-132.
- [19] Kanema J.M., Eid J., & Taibi S. (2016). Shrinkage of earth concrete amended with recycled aggregates and superplasticizer: Impact on mechanical properties and cracks. *Materials & Design*, 109, 378-389.
- [20] Ameer L.I., Hattab M. (2017). Crack initiation and propagation of clay under indirect tensile strength test by bending related to the initial suction. *ATMSS 2017*. [https://doi.org/10.1007/978-3-319-52773-4\\_19](https://doi.org/10.1007/978-3-319-52773-4_19)
- [21] Tang, C.S., Shi, B., Liu, C., Zhao, L., Wang, B.J., 2008. Influencing factors of geometrical structure of surface shrinkage cracks in clayey soils. *Engineering Geology* 101,204–217.
- [22] Zeng, H., Tang, C. S., Cheng, Q., Inyang, H. I., Rong, D. Z., Lin, L., & Shi, B. (2019). Coupling effects of interfacial friction and layer thickness on soil desiccation cracking behavior. *Engineering Geology*, 260, 105220.
- [23] Hild F. & Roux S. (2006), Digital Image Correlation: from Displacement Measurement to Identification of Elastic Properties - a Review. *Strain*, 42: 69-80.
- [24] Sutton, M. A., Wolters, W. J., Peters, W. H., Ranson, W. F., & McNeill, S. R. (1983). Determination of displacements using an improved digital correlation method. *Image and vision computing*, 1(3), 133-139.
- [25] Wagne, B., Roux, S., & Hild, F. (2002). Spectral approach to displacement evaluation from image analysis. *The European Physical Journal Applied Physics*, 17(3), 247-252.

- [26] Réthoré J., Roux S., & Hild F. (2009). An extended and integrated digital image correlation technique applied to the analysis of fractured samples: The equilibrium gap method as a mechanical filter. *European Journal of Computational Mechanics*, 18(3-4), 285-306.
- [27] Wang, L. L., Zhang, G. Q., Hallais, S., Tanguy, A., & Yang, D. S. (2017). Swelling of shales: a multiscale experimental investigation. *Energy & Fuels*, 31(10), 10442-10451.
- [28] El Hajjar A., Eid J., Ouahbi T., Taibi S. (2019). Risk of damage and desiccation cracking of construction materials based on raw earth. *MATEC Web Conf. Volume 281*.
- [29] El Hajjar A., Eid J., Bouchemella S., Ouahbi T., Taibi S. (2019). Retrait et fissuration des sols argileux par dessiccation. *Academic Journal of Civil Engineering*, 36(1), 624-628.
- [30] Kanavaris, F., Azenha, M., Soutsos, M., & Kovler, K. (2019). Assessment of behaviour and cracking susceptibility of cementitious systems under restrained conditions through ring tests: A critical review. *Cement and Concrete Composites*, 95, 137-153.
- [31] Dong W., Zhou X., Wu Z., A fracture mechanics-based method for prediction of cracking of circular and elliptical concrete rings under restrained shrinkage, *Eng. Fract. Mech.* 131 (2014) 687–701.
- [32] Dong W., Zhou X., Wu Z. & Kastiukas G., Effects on specimen size on assessment of shrinkage cracking of concrete via elliptical rings: thin vs. thick, *Comput. Struct.* 174 (2016) 66–78.
- [33] Dong W., Zhou X., Wu Z., Xu B., Investigating crack initiation and propagation of concrete in restrained shrinkage circular/elliptical ring test, *Mater. Struct.* 50 (2017) 1–13.
- [34] Dong W., Zhou X., Wu Z., Luo H. and Kastiukas G., Quantifying the influence of elliptical ring geometry on the degree of restraint in a ring test, *Comput. Struct.* 207 (2018) 111–120.
- [35] Weiss, J., Lura, P., Rajabipour, F., & Sant, G. (2008). Performance of shrinkage-reducing admixtures at different humidities and at early ages. *ACI Materials Journal*, 105(5), 478.
- [36] AASHTO PP 34; AASHTO PP 34-99 and AASHTO PP 334-08 – Standard Method of Test for Estimating the Cracking Tendency of Concrete. American Association of State Highway and Transportation Officials, Washington DC, USA (2008)
- [37] ASTM C1581/C1581M-16; ASTM C1581-04 and ASTM C1581/C1581M-09a – Standard Test Method for Determining Age at Cracking and Induced Tensile Stress Characteristics of Mortar and Concrete under Restrained Shrinkage ASTM International, West Conshohocken, PA, USA (2016)
- [38] Moon, J. H., Rajabipour, F., Pease, B., & Weiss, J. (2006). Quantifying the influence of specimen geometry on the results of the restrained ring test. *Journal of ASTM international*, 3(8), 1-14.

- [39] See, H. T., Attiogbe, E. K., & Miltenberger, M. A. (2003). Shrinkage cracking characteristics of concrete using ring specimens. *Materials Journal*, 100(3), 239-245.
- [40] Hossain, A. B., & Weiss, J. (2004). Assessing residual stress development and stress relaxation in restrained concrete ring specimens. *Cement and Concrete Composites*, 26(5), 531-540.
- [41] Moon, J. H., & Weiss, J. (2006). Estimating residual stress in the restrained ring test under circumferential drying. *Cement and Concrete Composites*, 28(5), 486-496.
- [42] Abou Najm, M., Mohtar, R.H., Weiss, J., Braudeau, E. (2009). Assessing internal stress evolution in unsaturated soils. *Water Resources Research* 45.
- [43] Costa, S. (2010), "Study of Desiccation Cracking and Fracture Properties of Clay Soils," Ph.D. dissertation, Department of Civil Engineering, Monash University, Australia.
- [44] Amarisiri, A., B. Shannon, J. Kodikara, 2014. "Numerical modelling of desiccation cracking in a restrained ring test." *Canadian Geotechnical Journal* 51(1): 67-76.
- [45] Shannon B.M., Kodikara J., Rajeev P., 2015. The use of restrained ring test method for soil desiccation studies. *Geotech. Test J.* 38.
- [46] Bouchemella S., El Hajjar A., Verheecke A., Serbah H., Ouahbi T., Taibi S. (2018). Etude du retrait empêché d'un matériau argileux en utilisant le ring test. *Academic Journal of Civil Engineering*, 36(1), 575-578.
- [47] El Hajjar A., Ouahbi T., Eid J., Hattab M., Taibi S. (2020). Shrinkage cracking of unsaturated fine soils: new experimental device and measurement techniques. *Strain*. 2020;e12352. <https://doi.org/10.1111/str.12352>
- [48] Hejazi, S. M., Sheikhzadeh, M., Abtahi, S. M., & Zadhoush, A. (2012). A simple review of soil reinforcement by using natural and synthetic fibers. *Construction and building materials*, 30, 100-116.
- [49] R. Jamshidi, I. Towhata, H. Ghiassian & R. Tabarsa. Experimental evaluation of dynamic deformation characteristics of sheet pile retaining walls with fiber reinforced backfill. *Soil Dynamics and Earthquake Engineering*. Volume 30, Issue 6, June 2010, Pages 438-446.
- [50] Abtahi M, Ebadi F, Hejazi M, Sheikhzadeh M. On the use of textile fibers to achieve mechanical soil stabilization. In: 4th Int tex cloth des conf, Dubrovnik, Croatia; 5-8 October, 2008.
- [51] Hanafi I, Few C. Partial replacement of silica by white rice husk ash in natural rubber compounds: the effects of bond. *Iran Polym J* 1998; 7:255-61.
- [52] Harriette L. The potential of flax fibers as reinforcement for composite materials. Eindhoven (the Netherlands): Eindhoven University Press; 2004.

- [53] Segetin M, Jayaraman K, Xu X. Harakeke reinforcement of soil-cement building materials: manufacturability and properties. *Build Environ* 2007; 42:3066-79.
- [54] Cheah J, Morgan T. UKU: concept to construction using flax-fibre reinforced stabilised rammed earth. In: 11th Int confe non-conv mat and tech; 6-9 September, Bath, UK, 2009.
- [55] Viswanadham, B. V. S., Jha, B. K., & Pawar, S. N. (2010). Influence of geofibers on the flexural behavior of compacted soil beams. *Geosynthetics International*, 17(2), 86-99.
- [56] Divya, P. V., Viswanadham, B. V. S., & Gourc, J. P. (2014). Evaluation of tensile strength-strain characteristics of fiber-reinforced soil through laboratory tests. *Journal of Materials in civil Engineering*, 26(1), 14-23.
- [57] Chaduvula, U., Viswanadham, B. V. S., & Kodikara, J. (2017). A study on desiccation cracking behavior of polyester fiber-reinforced expansive clay. *Applied Clay Science*, 142, 163-172.
- [58] Chebbi, M., Guiras, H., & Jamei, M. (2020). Tensile behaviour analysis of compacted clayey soil reinforced with natural and synthetic fibers. *European Journal of Environmental and Civil Engineering*, 24(3), 354-380.
- [59] Hattab, M., Hammad, T., & Fleureau, J. M. (2015). Internal friction angle variation in a kaolin/montmorillonite clay mix and microstructural identification. *Géotechnique*, 65(1), 1-11.
- [60] Fleureau, J. M., Kheirbek-Saoud, S., Soemitro, R., Taibi, S., 1993. Behavior of clayey soils on drying-wetting paths. *Canadian geotechnical journal*, 30(2), 287-296.
- [61] International Digital Image Correlation Society, Jones, E.M.C., Iadicola, M.A., 2018. A Good Practices Guide for Digital Image Correlation. <https://doi.org/10.32720/idics/gpg.ed1/print.format>
- [62] Schreier, H., Orteu, J. J., & Sutton, M. A. (2009). *Image correlation for shape, motion and deformation measurements: Basic concepts, theory and applications (Vol. 1)*. Boston, MA: Springer-Verlag US.